axioms

MDPI

Article

Effect of Heat/Mass Transfer and Magnetic Field on Peristaltic Flow of Rabinowitsch Fluid Through a Symmetric Inclined Channel with Thermal Radiation

Hanan S. Gafel and Luluah G. Albugami *

Department of Mathematics and Statistics, Taif University, Taif P.O. Box 11099, Saudi Arabia; h.gafal@tu.edu.sa
* Correspondence: s44580268@students.tu.edu.sa

Abstract

This study analyzes and explores the influence of multiple physical mechanisms—namely the influences of heat and mass transfer, thermal radiation, and magnetic field effects on the peristaltic transport of a Rabinowitsch-type non-Newtonian fluid within an inclined channel. To accurately represent the intricate behavior of the fluid under these coupled physical phenomena, a nonlinear model was formulated that integrates thermal, magnetic, and radiative forces into its framework. The given coupled differential equations are transformed into ordinary differential equations (ODEs). Using assumptions of long-wavelength and low-Reynolds-number approximations, the governing equations were significantly simplified. The resulting set of equations was solved analytically using Mathematica, subject to appropriate boundary conditions for velocity, temperature, and concentration. Graphs for velocity, temperature and concentration are illustrated. Thermal radiation was incorporated into the energy equation via the Rosseland approximation, thereby enabling a more accurate characterization of heat transport within the system. Moreover, the rate of heat and mass transfer for different variables was also examined. These findings are essential for the progression of advanced fluid transport systems in biomedical engineering, chemical processing, and energy generation, improving the design and management of non-Newtonian fluid dynamics.

Keywords: magnetic field; heat and mass transfer; thermal radiation; peristaltic transport; inclined conduit; Rabinowitsch-type non-Newtonian fluid model

MSC: 76A05; 76W05; 76Z05; 76R10

Check for updates

Academic Editor: Gabriella Bretti

Received: 5 April 2026
Revised: 18 May 2026
Accepted: 25 May 2026
Published: 4 June 2026

Copyright: © 2026 by the authors. Licensee MDPI, Basel, Switzerland. This article is an open access article distributed under the terms and conditions of the Creative Commons Attribution (CC BY) license.

1. Introduction

During the last few years, peristaltic transport has been the focus of many research studies because of its broad scope of application both in physiological processes and in industrial processes. This principle plays an important role in the transport of many biological fluids in animal and human bodies such as the transport of urine from the kidney to the bladder, food mixing and chyme movement in the gastrointestinal tract, transport of spermatozoa in the efferent ducts of the male reproductive tract and cervical canal, movement of eggs in the fallopian tube, swallowing of food through the esophagus, cilia movement and blood circulation in small blood vessels and movement of lymphatic fluids in lymphatic vessels. Moreover, the peristaltic mechanism has found many applications for fluid mechanics in engineering like high solid slurries, noxious fluid in nuclear industries,

hose pumps, heart-lung machines, roller pumps, blood pumps and dialysis machines. A few experimental and theoretical attempts were carried out to understand the peristaltic mechanism under different conditions. Abd-Alla et al. [1] investigated peristaltic transport within a nanofluid flowing through a ciliated tube, emphasizing its role in improving the system's heat and mass transfer efficiency. On the same note, Abd-Alla et al. [2] also examined the use of a peristaltic pump to study the behavior of heat and mass transfer of a fractional second-grade fluid that was flowing through a porous medium in a tube and showed the interactions between the kinematic and thermal properties of the fluid. These experiments put great emphasis on the importance of the porous medium effect because the introduction of the porous medium brings about an increased level of complexity on the peristaltic flow by creating more resistance forces and leakage, varying the pressure–velocity relationship. Knowledge of thermal properties, mass, and viscosity is thus important for physiological and engineering uses in the building of complicated peristaltic flow models.

Alrashdi [3] examined the peristaltic flow of the nanofluids and hybrid nanofluids in asymmetric channels with reference to heat transfer applications. The paper formulated mathematical models to identify the impacts of thermal properties, porosity, Darcy number, Hall currents, and magnetic fields on the velocity, pressure distribution, rheological behavior, and flow patterns in magnetohydrodynamic (MHD)-based studies.

In line with this, Bilal et al. [4] conducted studies on peristaltic flows of hybrid nanofluids and laid emphasis on the interaction of thermal and magnetic influence on asymmetric conduits. Chen et al. [5] studied the flow and transport of biological vascular systems both physiologically and chemically. The research was aimed at examining the flow pattern, material transport, and chemical reactions in the blood vessels, with a particular focus on the extent to which the structural properties of the blood vessels systems affect the velocity, pressure and solutes distribution. Moreover, the review offered an integrated perspective on the modeling, analysis, and experimental studies toward understanding peristaltic dynamics and transport in the human body as well as the significance of applying concepts of physiology and chemical engineering in the design and simulation of models. The peristaltic mechanism underlies many biological functions, such as the transport of chyme along the gastrointestinal tract, the passage of urine through the ureters, and fluid transport in reproductive channels. In this regard, Esser et al. [6] demonstrated how living organisms use the peristaltic principle to transport fluids efficiently and quietly and how the same principle can be applied in engineering pumps to convey sensitive fluids without direct contact with mechanical components, offering additional benefits such as reduced wear, lower maintenance, and consistent flow regulation. Heat and mass transfer in a second-grade fluid passing through a porous media under the long-wavelength-approximation, low-Reynolds-number model was studied by Farooq et al. [7], who showed that buoyancy and wall slide significantly affect temperature distribution. He applied this method to electro-osmotic Sutterby nanofluids, showing that adding thermophoretic and Brownian effects improves energy dissipation. More generally, these investigations indicate that pumping efficiency, trapping mechanisms, and energy transfer in peristaltic systems are significantly influenced by the interaction of magnetohydrodynamics (MHD), pore resistance, and non-Newtonian rheology.

Peristaltic analyses in porous channels also draw from both classical and contemporary theoretical frameworks. Hasan et al. [8] obtained flux–pressure relations in the peristaltic pumping in slim orifices with permeable walls through the combination of lubrication theory and the law of Darcy. Khan et al. [9] studied peristaltic behavior in channels which are asymmetric and have magnetic fields and porous media, showing that porosity and strength of the magnetic field have a great effect on trapping and pressure increase. Magdy et al. [10] studied the influence of wall slip and heat transfer on particle-laden fluid

magnetohydrodynamic (MHD) peristaltic flow. They created a mathematical formulation to determine dynamic velocity, pressure field, and energy transport focusing on the effect of wall slip and turbulent particles on thermal and hydrodynamic properties of the flow.

Similarly, Magdy et al. [11] examined the influence of a magnetic field and heat transfer on peristaltic transport in an asymmetrically inclined channel considering the wall slide. The analysis of the velocity, pressure and heat transfer properties of peristaltic flow pointed to the impact of slip, magnetic field and channel asymmetry on the dynamics of peristaltic flow. Mohamed et al. [12], in their study of the magnetohydrodynamic (MHD) peristaltic flow of viscoelastic nanofluids through porous asymmetric channels, discovered that with a stronger magnetic field, uniformity of flow is enhanced, and pressure drop is reduced.

Hayat et al. [13] investigated the influence of thermal radiation on peristaltic flow of non-Newtonian fluids and reported significant effects on temperature distribution and heat transfer characteristics. Akbar et al. [14] examined magnetohydrodynamic peristaltic flow with thermal radiation and showed that radiation and magnetic field strongly influence velocity and thermal behavior. Ellahi et al. [15] studied the impact of thermal radiation on peristaltic transport and demonstrated that radiative effects play an important role in heat and mass transfer processes.

In contrast, Sanil et al. [16] investigated the peristaltic motion of non-Newtonian Ree–Eyring fluid with variable fluid properties, with a focus on maximization of the entropy production to minimize the loss of energy to heat transfer and viscous dissipation. The results revealed that the thermodynamic and flow performance of the fluid can be significantly improved by changing the viscosity and thermal properties.

To gain a superior understanding of the intricate peristaltic and convective processes and to develop superior thermal and biological flow systems, our work valuates the importance of integrating thermal-magnetic manipulation and entropy-based modeling. To understand the effects of the characteristics of wall permeability and porous medium on the effectiveness of the pumping process and on the flow characteristics, the study conducted by Takagi et al. [17] investigated peristaltic pumping in a porous conduit.

The mathematical model of the interaction of peristaltic waves with the fluid flow and the porous media through the Stokes and Darcy equations was employed by the scientists. Their observations showed that although the walls absorb or leak fluid leading to observable change in the net flow rate, increased permeability leads to reduced pumping pressure required and velocity distribution within the conduit.

Overall, this piece of work provides information about peristaltic transport in porous surfaces, and its implications in chemical engineering, environmental engineering and bioengineering (including fluid flow in tissues). Other studies [18–24] were primarily aimed at investigating the effects of peristaltic and thermal flow in non-Newtonian and nanofluids due to the action of magnetic fields, convective mechanisms, and various fluid characteristics. They focused on entropy creation, Joule heating, pressure diffusion and velocity distribution in different curved systems, such as stenosed arteries and inclined channels. Moreover, the thermal and flow performance of the fluid was also assessed by other studies through complex computational techniques, e.g., artificial neural networks. Vaidya et al. [25] employed a modified Darcy law to investigate peristaltic transport of non-Newtonian fluid with a strong focus on the channel permeability and its influence on velocity and pressure distribution. Vlahovska [26] focused on the electrohydrodynamics of drops and vesicles, their behavior under electric fields and the resulting effects on shape formation and stability. Meanwhile, Zhang et al. [27] concentrated on non-linear interactions among stresses, thermal movement and particle transport during the research of the liaison movement of particles, and fluid under peristaltic flow with thermal impact and mass transfer. In recent years, researchers have extensively focused on the heat/mass transfer

and magnetic field on peristaltic flow of Rabinowitsch fluid through a symmetric inclined channel (for example in [28–37] and several references therein). A literature survey reveals that a study on the effect of radiation, and heat and mass generation/absorption [32,33] for peristalsis of Rabinowitsch fluid has not been attempted yet. Here, we examined the radiative peristaltic transport of Rabinowitsch fluid. Velocity features are considered along channel walls. Heat and mass transfer force and Hartmann number impacts are also recorded in this study. The governing equations were derived under the assumptions of a large wavelength and a small Reynolds number. The resulting set of equations was solved analytically using Mathematica. The graphical results highlight how the main parameters influence the velocity field, temperature profile, concentration level, and heat transfer rate.

2. Materials and Methods

This study investigated the behavior of an incompressible Rabinowitsch fluid undergoing peristaltic motion within a uniform inclined channel. The channel walls in this case are symmetric and have a width of $2a$. Cartesian coordinates x and y were selected in such a manner so that it is assumed horizontally along a wave's propagation and y is taken into account perpendicularly. The fluid flowed along the channel walls, driven by sinusoidal wave trains with wavelength λ and constant speed c, where b represents the wave amplitude and t denotes the wave duration. The sinusoidal equations outlined below are employed to identify the geometry of deformable walls as depicted in Figure 1 [38].

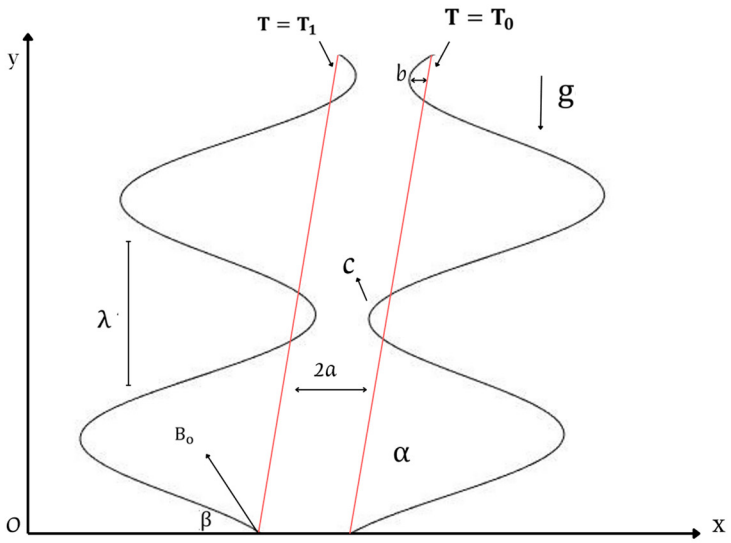


Figure 1. Geometric description of the model.

$$\overline{Y} = \overline{H}\,(\overline{X}, \overline{t}) = a + b\,sin\frac{2\pi}{\lambda}(\overline{X} - \overline{ct}), \tag{1}$$

The governing equations for the flow are:

$$\frac{\partial \overline{U}}{\partial \overline{X}} + \frac{\partial \overline{V}}{\partial \overline{Y}} = 0, \tag{2}$$

$$\rho\left[\frac{\partial \bar{U}}{\partial \bar{t}} + \bar{U}\frac{\partial \bar{U}}{\partial \bar{X}} + \bar{V}\frac{\partial \bar{U}}{\partial \bar{Y}}\right] = -\frac{\partial \bar{P}}{\partial \bar{X}} + \frac{\partial \bar{S}_{\overline{XX}}}{\partial \bar{X}} + \frac{\partial \bar{S}_{\overline{XY}}}{\partial \bar{Y}} + \rho g sin\xi - \sigma B_{\circ}^{2} cos\,\alpha(\bar{U}cos\alpha - \bar{V}sin\alpha), \tag{3}$$

$$\rho\left[\frac{\partial \bar{V}}{\partial \bar{t}} + \bar{U}\frac{\partial \bar{V}}{\partial \bar{X}} + \bar{V}\frac{\partial \bar{V}}{\partial \bar{Y}}\right] = -\frac{\partial \bar{P}}{\partial \bar{Y}} + \frac{\partial \bar{S}_{\overline{YX}}}{\partial \bar{X}} + \frac{\partial \bar{S}_{\overline{YY}}}{\partial \bar{Y}} - \rho g cos\xi - \sigma B_{\circ}^{2} cos\alpha(\bar{U}cos\alpha - \bar{V}sin\alpha), \tag{4}$$

The heat conduction equation is as follows:

$$\rho C_P\left[\frac{\partial \overline{T}}{\partial \overline{t}}+\overline{U}\frac{\partial \overline{T}}{\partial \overline{X}}+\overline{V}\frac{\partial \overline{T}}{\partial \overline{Y}}\right]=K\left(\frac{\partial^2 \overline{T}}{\partial \overline{X}^2}+\frac{\partial^2 \overline{T}}{\partial \overline{Y}^2}\right)+\overline{S}_{\overline{X}\overline{X}}\frac{\partial \overline{U}}{\partial \overline{X}}+Q_\circ-\frac{\partial q_r}{\partial \overline{Y}}, \tag{5}$$

The concentration equation is as follows:

$$\left[\bar{U}\frac{\partial \bar{C}}{\partial \bar{X}}+\bar{V}\frac{\partial \bar{C}}{\partial \bar{Y}}\right]=D_m\left[\frac{\partial^2 \bar{C}}{\partial \bar{X}^2}+\frac{\partial^2 \bar{C}}{\partial \bar{Y}^2}\right]+\frac{D_m K_T}{T_m}\left[\frac{\partial^2 \bar{T}}{\partial \bar{X}^2}+\frac{\partial^2 \bar{T}}{\partial \bar{Y}^2}\right], \tag{6}$$

By applying the Rosseland diffusion approximation, the radiative flux is expressed as follows:

$$q_r=-\frac{4\overline{\sigma}}{3\overline{k}}\frac{\partial \overline{T}^4}{\partial \overline{y}}, \tag{7}$$

It is important to note that this model considers the optically thick radiation limit. It is assumed that the temperature variations within the flow are sufficiently small such that $\overline{T}^4$ can be approximated as a linear function of temperature. This is achieved by expanding $\overline{T}^4$ using a Taylor series around the reference temperature T_0 as follows:

$$\overline{T}^4=T_0^4+4T_0^3\left(\overline{T}-T_0\right)+6T_0^2\left(\overline{T}-T_0\right)^2+\cdots$$

By neglecting the higher-order terms (second order onwards), we arrive at

$$\overline{T}^4\approx -3T_0^4+4T_0^3. \tag{8}$$

By taking the derivative of Equation (7) with respect to $\overline{Y}$ and using Equation (8), we obtain

$$\frac{\partial q_r}{\partial \overline{Y}}=-\frac{16\overline{\sigma}T_0^3}{3\overline{k}}\frac{\partial^2 \overline{T}}{\partial \overline{Y}^2}, \tag{9}$$

In the laboratory frame $(\bar{X},\bar{Y})$ the flow is unsteady. However, if observed in a coordinate system moving at the wave speed c (wave frame) $(\bar{x},\bar{y})$, it can be treated as steady. Transforming variables from the laboratory into the wave frames comprises:

$$\bar{x}=\bar{X}-c\bar{t},\quad \bar{y}=\bar{Y},\quad \bar{u}=\bar{U}-c,\ \bar{v}=\bar{V},\bar{p}=\bar{P},\quad \bar{c}=c,\ \overline{T}=T, \tag{10}$$

We let $\overline{u}$ and $\overline{v}$ denote the velocity components in the wave frame $(\bar{x},\bar{y})$, $\overline{p}$ the pressure, and $\overline{P}$ the corresponding quantity in the fixed reference frame.

The following non-dimensional variables and parameters are then introduced for the flow:

$$\begin{gathered}
x=\frac{\bar{x}}{\lambda},y=\frac{\bar{y}}{a},t=\frac{c\bar{t}}{\lambda},p=\frac{a^2\bar{p}}{c\mu\lambda}\\
\delta=\frac{a}{\lambda},u=\frac{\bar{u}}{c},v=\frac{\bar{v}}{c\delta},Re=\frac{\rho ca}{\mu},\\
\delta_{ij}=\frac{a\bar{\delta}_{ij}}{c\mu},\ \theta=\frac{\overline{T}-T_0}{T_1-T_0},\ \beta=\frac{a^2\overline{Q}}{K(T_1-T_0)},\\
B_i=\frac{ah}{K},\ M=B_o a\sqrt{\frac{\sigma}{\mu}},\quad \Theta=\frac{\overline{C}-C_0}{C_1-C_0},\ R=\frac{16\overline{\sigma}T_0^3}{3\overline{k}K},
\end{gathered} \tag{11}$$

where ξ is the angle of inclination of the channel, β is the heat source/sink parameter, g is the gravity field, β_1 is the heat transfer coefficient, and δ is the wave number, with the following formulas representing the stress components:

$$\bar{S}_{\overline{XX}} = \frac{2\mu}{1+\lambda_1}\left[1+\lambda_2\left[\bar{U}\frac{\partial}{\partial\bar{X}}+\bar{V}\frac{\partial}{\partial\bar{Y}}\right]\right]\frac{\partial\bar{U}}{\partial\bar{X}},$$
$$\bar{S}_{\overline{XY}} = \frac{\mu}{1+\lambda_1}\left[1+\lambda_2\left[\bar{U}\frac{\partial}{\partial\bar{X}}+\bar{V}\frac{\partial}{\partial\bar{Y}}\right]\right]\left[\frac{\partial\bar{U}}{\partial\bar{Y}}+\frac{\partial\bar{V}}{\partial\bar{X}}\right], \quad (12)$$
$$\bar{\delta}_{\overline{YY}} = \frac{2\mu}{1+\lambda_1}\left[1+\lambda_2\left[\bar{U}\frac{\partial}{\partial\bar{X}}+\bar{V}\frac{\partial}{\partial\bar{Y}}\right]\right]\frac{\partial\overline{V}}{\partial\overline{Y}},$$

2.1. Solution to the Problem

Using the above transformations (10) along with the non-dimensional variables (11), the governing Equations (2)–(6) are reduced to:

$$\left(\frac{\partial u}{\partial x}+\frac{\partial v}{\partial y}\right)=0, \quad (13)$$

$$Re\delta\left[u\frac{\partial u}{\partial x}+v\frac{\partial u}{\partial y}\right]=-\frac{\partial p}{\partial x}+\beta_2\frac{\partial^2 u}{\partial y^2}+\gamma sin\xi-M^2 cos\alpha(ucos\alpha-vsin\,\alpha), \quad (14)$$

$$Re\delta^3\left[u\frac{\partial v}{\partial x}+v\frac{\partial v}{\partial y}\right]=-\frac{\partial p}{\partial y}+\beta_2\delta^2\frac{\partial^2 u}{\partial x\partial y}-\delta\gamma cos\xi-\delta M^2 cos\alpha(ucos\alpha-v\delta sin\alpha), \quad (15)$$

$$\frac{C_p\rho ac}{k}\delta\left[u\frac{\partial\theta}{\partial x}+v\frac{\partial\theta}{\partial y}\right]=\left[\delta^2\frac{\partial^2\theta}{\partial x^2}+\frac{\partial^2\theta}{\partial y^2}\right]+\beta+R\frac{\partial^2\theta}{\partial y^2}, \quad (16)$$

$$c\delta a\left[u\frac{\partial\Theta}{\partial x}+v\frac{\partial\Theta}{\partial y}\right]=D_m\left[\delta^2\frac{\partial^2\Theta}{\partial x^2}+\frac{\partial^2\Theta}{\partial y^2}\right]+\frac{D_m K_T}{T_m}\frac{(T_1-T_o)}{(c_1-c_0)}\left[\delta^2\frac{\partial^2\theta}{\partial x^2}+\frac{\partial^2\theta}{\partial y^2}\right], \quad (17)$$

where

$$S_{xx} = \frac{2\delta}{1+\lambda_1}\left[1+\frac{\lambda_2\delta c}{a}\left[u\frac{\partial}{\partial x}+v\frac{\partial}{\partial y}\right]\right]\frac{\partial u}{\partial x},$$
$$S_{xy} = \frac{1}{1+\lambda_1}\left[1+\frac{\lambda_2\delta c}{a}\left[u\frac{\partial}{\partial x}+v\frac{\partial}{\partial y}\right]\right]\left[\frac{\partial u}{\partial y}+\delta^2\frac{\partial v}{\partial x}\right], \quad (18)$$
$$S_{yy} = \frac{2\delta}{1+\lambda_1}\left[1+\frac{\lambda_2\delta c}{a}\left[u\frac{\partial}{\partial x}+v\frac{\partial}{\partial y}\right]\right]\frac{\partial v}{\partial y},$$

By simplifying and applying the long-wavelength and low-Reynolds-number assumptions, Equations (13)–(17) reduce to:

$$-\frac{\partial p}{\partial x}+\beta_2\frac{\partial^2 u}{\partial y^2}+\gamma sin(\xi)-M^2 ucos^2(\alpha)=0, \quad (19)$$

$$\frac{\partial p}{\partial y}=0, \quad (20)$$

$$(1+R)\frac{\partial^2\theta}{\partial y^2}+\beta=0, \quad (21)$$

$$\frac{\partial^2\Theta}{\partial y^2}+\frac{K_T}{T_m}\frac{T_o}{c_o}\frac{\partial^2\theta}{\partial y^2}=0, \quad (22)$$

The corresponding dimensionless boundary conditions are given by:

$$u=-1, \quad \theta=0, \quad \Theta=0 \quad \text{at} \quad y=0, \quad (23)$$

$$u = -1, \quad \theta = 1, \quad \Theta = 1 \text{ at } \quad y = h = y = h = 1 + \varepsilon\, sin(2\pi x),$$

where $h = 1 + \varepsilon\, sin(2\pi x)$.

The solutions of Equations (19)–(22), under the boundary conditions specified in (23), can be written as

$$u = e^{a_3 h} e^{-a_3 y}(b_{33} - 1) - b_{33}, \tag{24}$$

$$\theta = csc\left(h\sqrt{\beta}\right) sin\left(y\sqrt{\beta}\right) \tag{25}$$

$$\Theta = \left[\frac{1}{h} + \frac{A_{11}}{h\beta}\, sin\left(h\sqrt{\beta}\right) y - \frac{A_{11}}{\beta}\, sin\left(y\sqrt{\beta}\right)\right], \tag{26}$$

$$\frac{\partial p}{\partial x} = \beta_2 \frac{\partial^2 u}{\partial y^2} + \gamma sin(\xi) - M^2 u cos^2(\alpha), \tag{27}$$

$$\Delta p_\lambda = \int_0^{2\pi} \frac{dp}{dx} dx, \tag{28}$$

$$F_\lambda = \int_0^{2\pi} (-h^2) \frac{dp}{dx} dx, \tag{29}$$

where

$$\beta_2 = \frac{a}{c\mu(1 + \lambda_1)}, \ \gamma = \frac{a^2 \rho g}{c\mu}, \tag{30}$$

$$a_3 = \frac{Mcos(\alpha)}{\sqrt{\beta_2}}, \ A_{11} = \frac{K_T T_0 \beta csc\left(h\sqrt{\beta}\right)}{T_m c_0}, \ b_{33} = \frac{sec^2(\alpha)(p_1 - \gamma\, sin(\xi)}{M^2},$$

where λ_2 is the retardation time, R is the thermal radiation, and c_0 is the reference concentration.

2.2. Validity of the Model

When the peristaltic transport of a Rabinowitsch-type non-Newtonian fluid within an inclined channel (which is illustrated by thermal radiation, heat source and Hatman number) is ignored, the peristaltic transport of a Rabinowitsch-type within an inclined channel is obtained and the results agree with Abdelhafez et al. [37]. When the mass transfer (which is illustrated by concentration C) is ignored, the peristaltic transport of a Rabinowitsch-type fluid is obtained and the results agree with Elmhedy et al. [33].

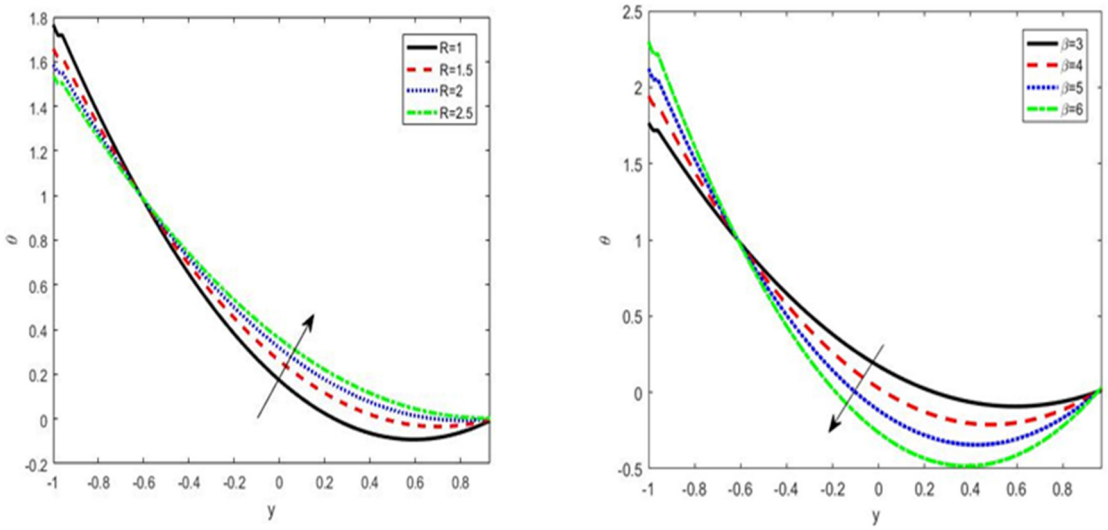
3. Results and Discussion

The primary aim of this research is to examine how an inclined magnetic field, together with heat and mass transfer, influences the peristaltic motion of a Rabinowitsch fluid flowing through an inclined symmetric channel. The analysis considers the combined effects of thermal radiation R, heat source or sink β, gravitational parameter γ, aligned magnetic field α, and the inclination angle of the asymmetric channel relative to the vertical ξ.

In the preceding section, the behavior of an electrically conducting Rabinowitsch fluid within an inclined wavy channel under the action of an oblique magnetic field was investigated. The effects of key governing parameters on the temperature θ, concentration Θ, velocity u, pressure gradient $\frac{dp}{dx}$, pressure rise ΔP_λ, and frictional forces F_λ, have been thoroughly analyzed. The corresponding results are illustrated in Figures 2–7.

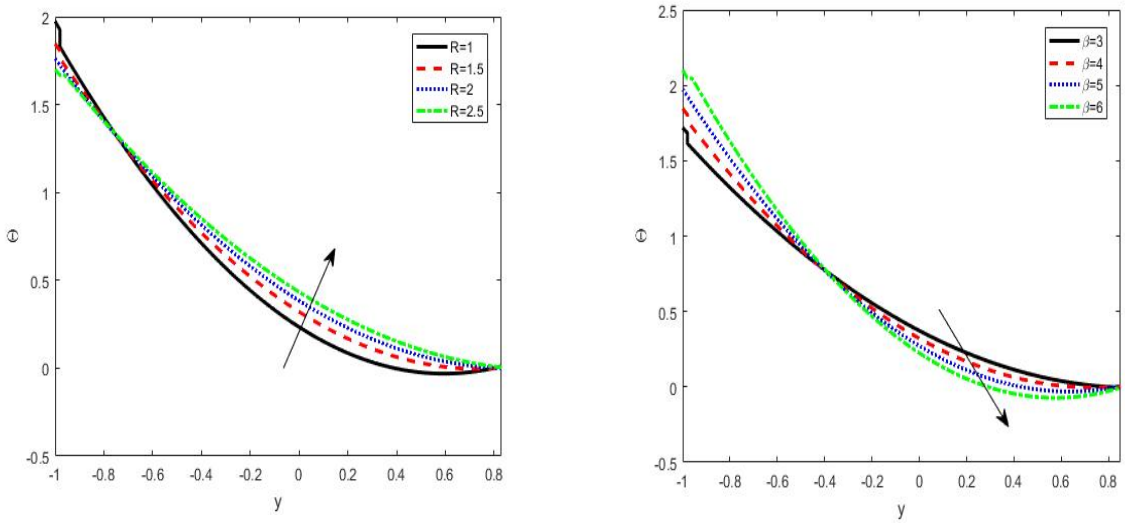
Figure 2 illustrates the effects of the thermal radiation parameter R and the heat source/sink parameter β on the temperature distribution θ.

Figure 2a shows that the temperature increases with increasing values of the thermal radiation parameter R due to the enhancement of radiative heat flux within the fluid, which elevates the overall thermal energy.



(**a**) (**b**)

Figure 2. Variation in the temperature distribution θ with respect to y for different values of (**a**) the thermal radiation parameter R and (**b**) the heat source/sink parameter β.



(**a**) (**b**)

Figure 3. Variation in the concentration distribution Θ with respect to y for different values of (**a**) the thermal radiation parameter R and (**b**) the heat source/sink parameter β.

On the other hand, Figure 2b shows that the temperature decreases with increasing values of β, indicating that this parameter acts as a heat sink, removing thermal energy from the fluid and thereby reducing the temperature distribution.

Moreover, the temperature profiles exhibit smooth and continuous behavior across the channel and tend to converge toward fixed values at the boundaries, which is consistent with the imposed thermal boundary conditions.

These results are consistent with those reported by Abd-Alla et al. [2].

Figure 3 illustrates the variation in the concentration profile Θ with respect to the transverse coordinate y for different values of the thermal radiation parameter R and the heat source/sink parameter β.

Figure 3a shows that the concentration increases with increasing values of the thermal radiation parameter R, which can be attributed to the enhancement of thermal energy within the fluid. This increase in thermal energy promotes mass diffusion and particle transport, leading to a higher concentration distribution across the channel.

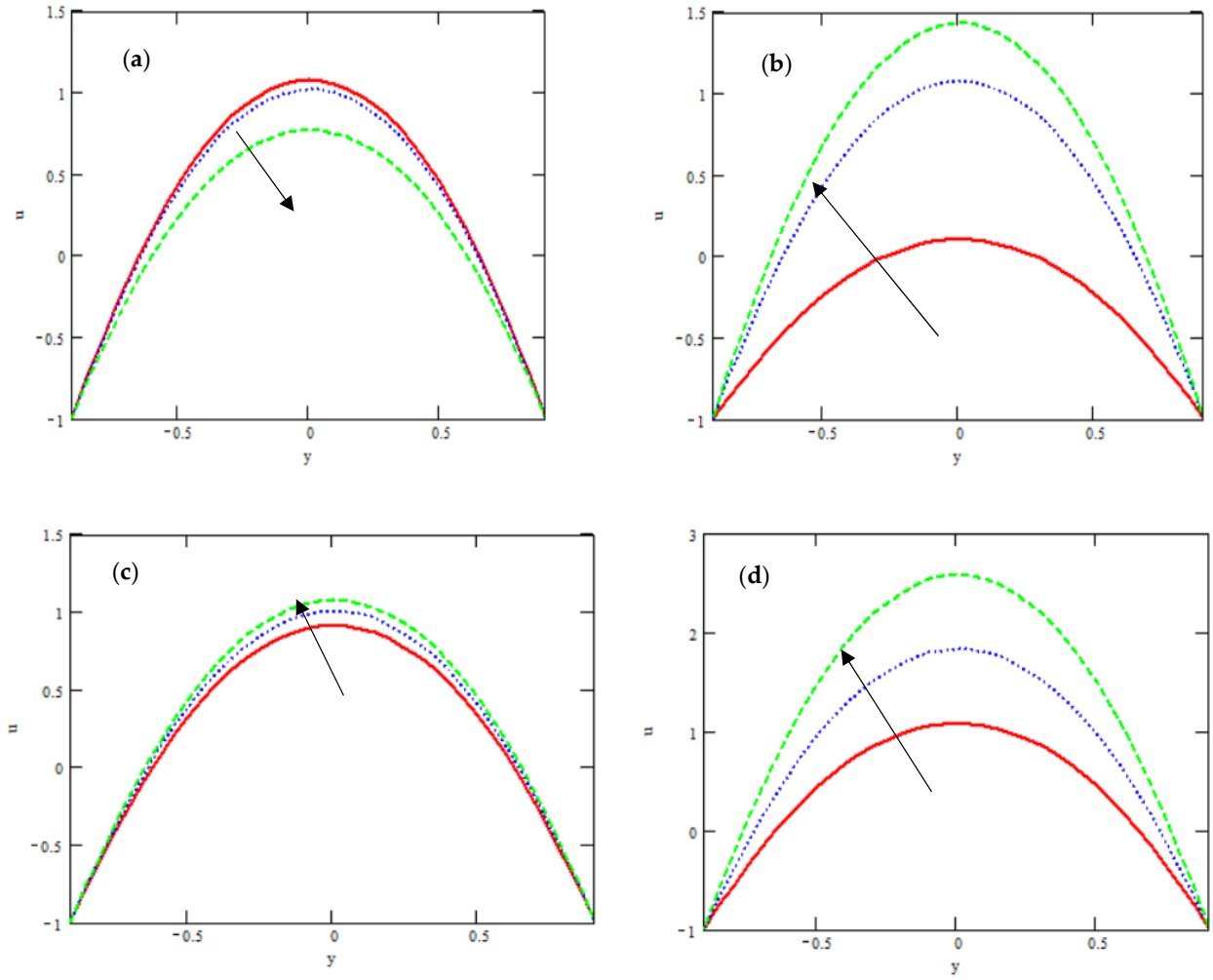
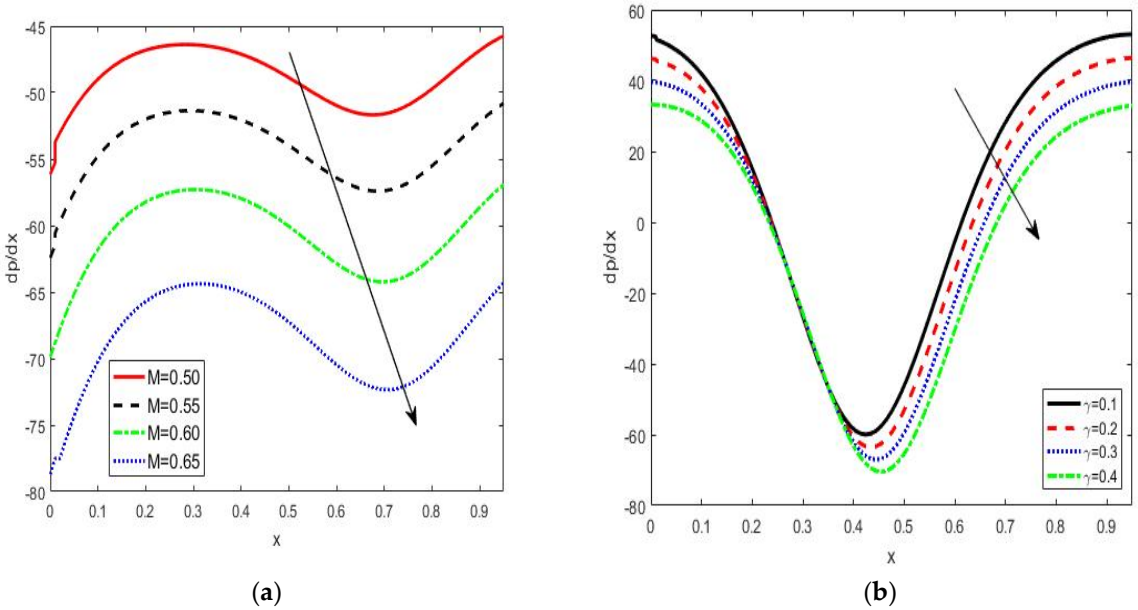


Figure 4. Variation in the velocity distribution u with respect to y for different values of (**a**) the Hartmann number M, (**b**) the channel inclination angle α, (**c**) the gravity field g, and (**d**) the ratio of relaxation to retardation times λ_1.



(**a**) (**b**)

Figure 5. Variation in the pressure gradient $\frac{dp}{dx}$ with respect to x for different values of (**a**) the Hartmann number M and (**b**) the gravitational parameter γ.

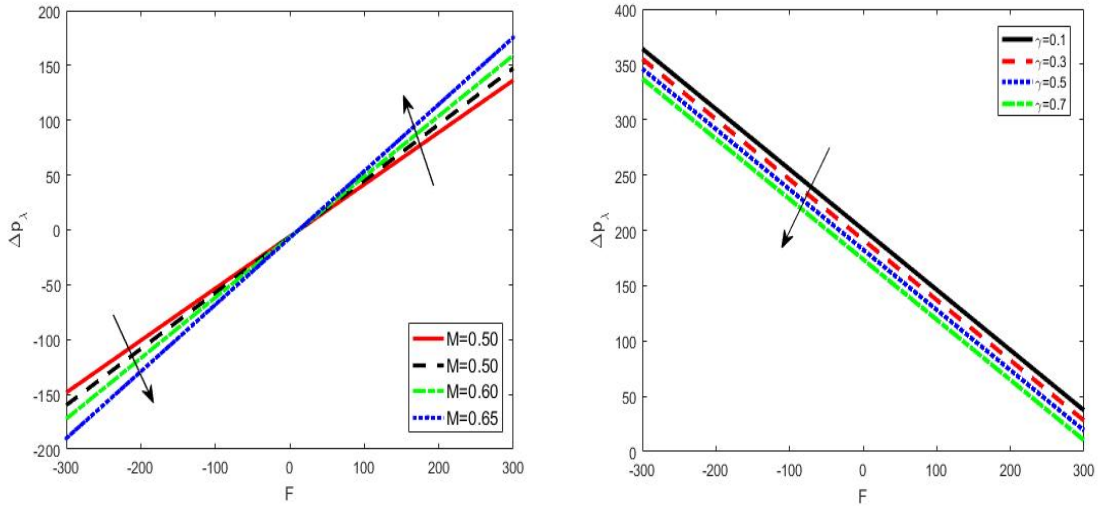


Figure 6. Variation in the pressure rise ΔP_λ with respect to the volume flow rate F for different values of (**a**) the Hartmann number M and (**b**) the gravitational parameter γ.

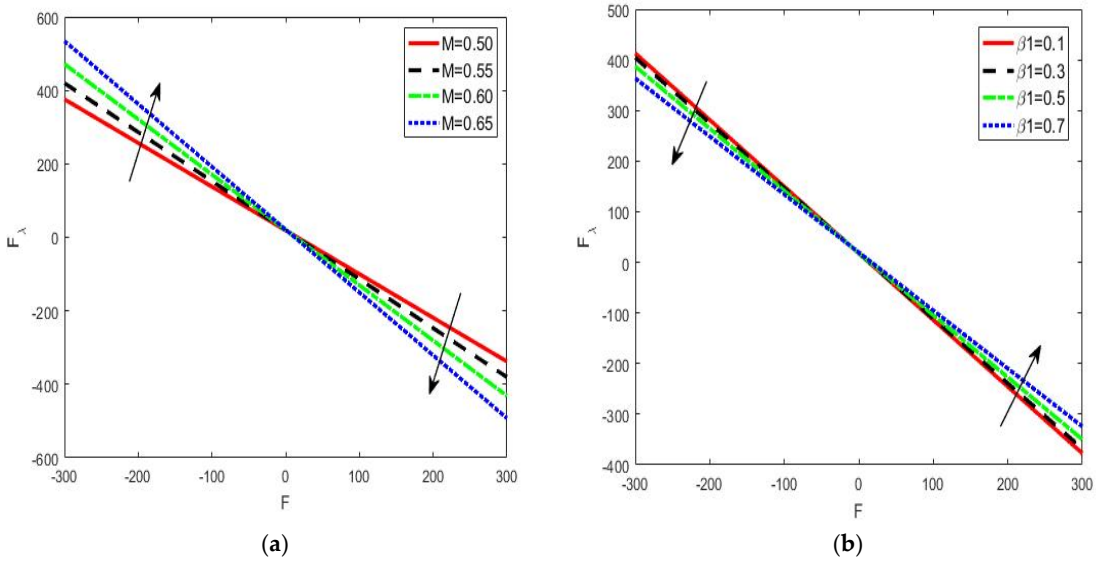


Figure 7. Variation in the friction force F_λ with respect to the volume flow rate F for different values of (**a**) the Hartmann number M and (**b**) the heat source/sink β.

On the other hand, Figure 3b shows that the concentration decreases with increasing values of β, indicating that the heat sink effect reduces the thermal energy within the fluid. This reduction in thermal energy weakens the mass diffusion process and limits particle transport, leading to a decrease in the concentration distribution.

Moreover, the concentration profiles exhibit smooth and continuous behavior across the channel and tend to converge toward fixed values at the boundaries, which is consistent with the imposed concentration boundary conditions.

These results are consistent with those reported by Abd-Alla et al. [2].

Figure 4 shows the variation in the axial velocity u with respect to the y-axis for different values of Hartmann number M, channel inclination angle α, gravity field g and the ratio of relaxation to retardation times λ_1. It is observed that the axial velocity decreases with increasing Hartmann number, while it increases with increasing channel inclination angle, gravity field and retardation and relaxation time. Moreover, the velocity profiles exhibit smooth and continuous behavior and satisfy the imposed boundary conditions

at the channel walls, confirming the physical validity of the solution. These results are consistent with those reported by Abd-Alla et al. [1].

Figure 5 illustrates the variation in the pressure gradient $\frac{dp}{dx}$ with respect to the axial coordinate x under the influence of the Hartmann number M and the gravitational parameter γ.

Figure 5a shows that the pressure gradient exhibits an oscillatory behavior throughout the entire range of x, which is primarily attributed to the peristaltic motion of the channel walls. It is also observed that an increase in the Hartmann number enhances the Lorentz force, leading to greater resistance to the flow and consequently higher pressure gradients.

In contrast, Figure 5b shows that the gravitational parameter modifies the pressure distribution by acting as an additional driving force along the flow direction.

Furthermore, it is observed that a relatively larger pressure gradient is required to maintain the same volumetric flow rate in the wider region of the channel, $x \in [0, 0.95]$. On the other hand, in the narrower region, $x \in [0.18, 0.58]$, a smaller pressure gradient is sufficient to sustain the same flow rate, particularly near the narrowest section around $x = 0.39$. This behavior is consistent with the physical characteristics of peristaltic transport.

These observations highlight the sensitivity of the pressure gradient to geometric variations in the channel, which is important in the design of efficient fluid transport systems operating under varying physical conditions.

Additionally, identifying regions of high sensitivity in the pressure gradient can help in designing more robust systems that perform consistently across a range of operating conditions, in agreement with [5].

Figure 6 illustrates the variation in the pressure rise ΔP_λ with respect to the volumetric flow rate F.

Figure 6a shows that the pressure rise varies linearly with the flow rate, particularly in the region $F \in (-300, 0)$. The pressure rise is defined as the pressure difference per wavelength, representing the ability of the peristaltic wave to drive the fluid along the channel.

Figure 6b shows that peristaltic pumping occurs within the region $-300 \leq F \leq 300$, while augmented pumping occurs when the flow is assisted by the wave motion, resulting in a larger pressure rise compared to the case of peristaltic pumping. The flow regimes can be classified based on the signs of F and ΔP_λ. The region where $F > 0$ and $\Delta P_\lambda < 0$ corresponds to augmented pumping, whereas the region where $F < 0$ and $\Delta P_\lambda > 0$ is known as retrograde or backward pumping, where the flow moves opposite to the peristaltic wave.

Thus, the flow behavior depends strongly on the direction of flow, where directional effects play a significant role in the mechanical response of the system. These results are in good agreement with those obtained by Magdy et al. [10,11].

Figure 7 illustrates the sensitivity of the governing system to variations in physical parameters, showing the variation in the frictional force with respect to the volumetric flow rate F for different values of the Hartmann number M and the heat source/sink parameter β.

Figure 7a shows that there exists a linear relationship between the frictional force and the volumetric flow rate. The frictional force increases with increasing values of the Hartmann number M in the negative flow region ($F < 0$), while it decreases in the positive flow region ($F > 0$), indicating that its behavior depends on the direction of flow.

Similarly, Figure 7b shows that the frictional force decreases with increasing values of the heat source/sink parameter β in the negative flow region ($F < 0$), while it increases in the positive flow region ($F > 0$), reflecting the reduction in the magnitude of frictional force.

Moreover, the frictional force exhibits an opposite trend compared to the pressure rise, highlighting the inverse relationship between these two physical quantities. This result is in good agreement with the results obtained in reference [11].

Streamline Pattern and Trapping Phenomenon

Trapping occurs when some streamlines split to enclose a bolus of fluid particles representing closed streamlines under certain conditions. Backward flow occurs when the entire flow is going in the opposite direction to the normal flow. Augmented flow occurs on the channel when the trapped bolus breaks up and there is some flow going in the forward direction.

Now, we consider the most interesting feature of peristaltic motion, which is the trapping of the flow, where streamlines split to trap a bolus in the wave frame; thus, the Hartmann number M is varied and a rich variety of flow patterns are observed. In Figure 8a, surprisingly, we observe that the trapping phenomenon occurs at $M = 0.5$. On the other hand, it is shown in Figure 8b that when the value of the Hartmann number increases at $M = 0.9$, there was a transition of the trapping phenomenon into backward flow. In addition, in Figure 9, it is shown that when the ratio of relaxation to retardation times λ_1 increased, the number of boluses increased due to a change in velocity distribution. This resulted in an increase in the size of the bolus trapped which describes the volume of the fluid that is bound by invariant closed streamlines. Also, the trapping phenomenon occurring at $\beta = 4$ resulted in an increase in the size of the bolus trapped which describes the volume of the fluid (Figure 10).

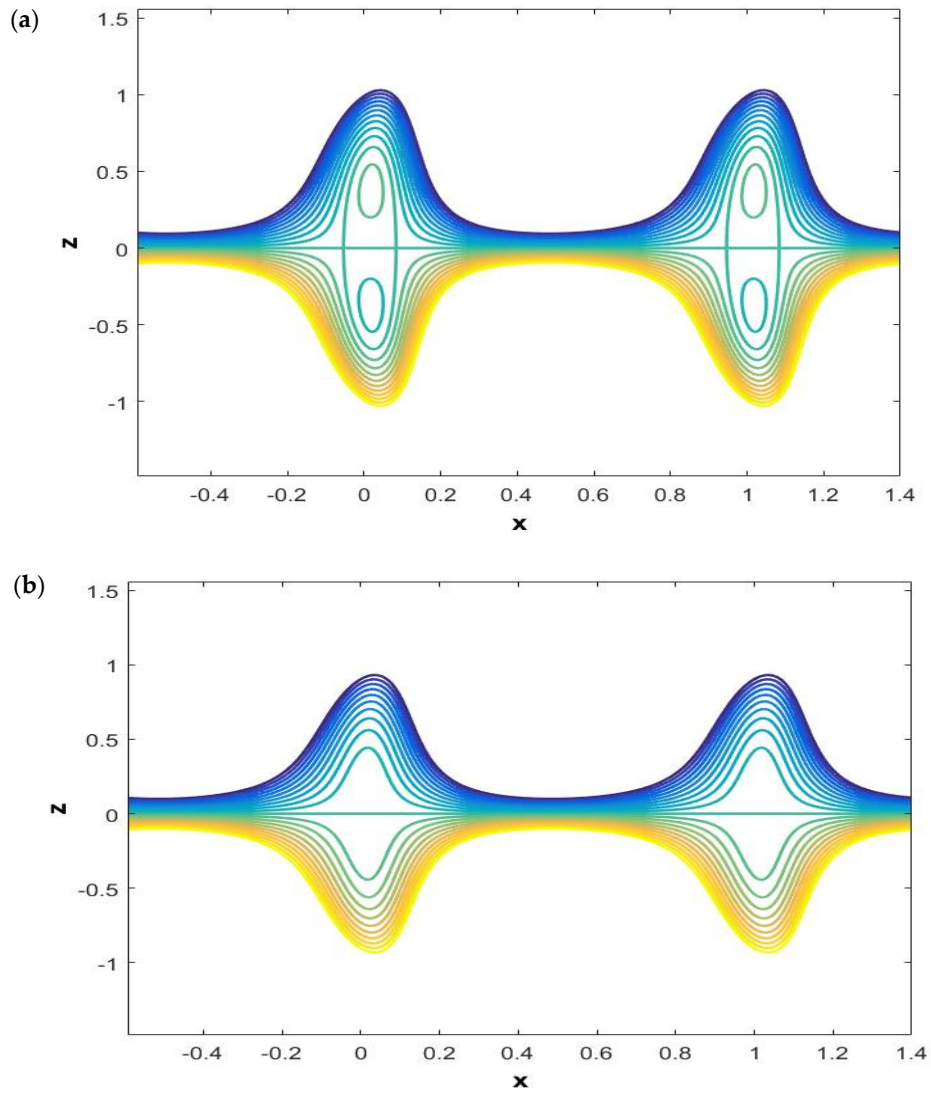


Figure 8. Different circumstances of flow correspond to different values of M. (**a**) The trapping phenomenon occurs at $M = 0.5$. (**b**) The backward flow occurs at $M = 0.9$.

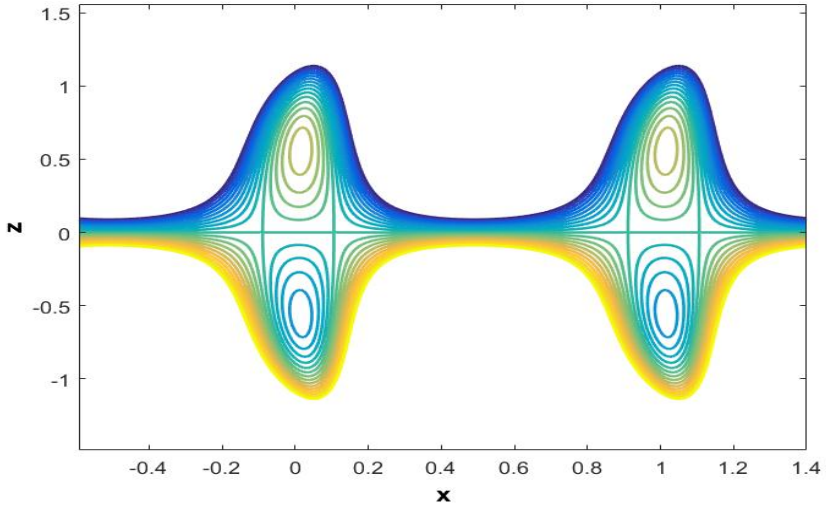


Figure 9. The trapping phenomenon occurs at $\lambda_1 = 1.5$ with increasing number of boluses such that there are symmetric boluses in the upper and lower channel.

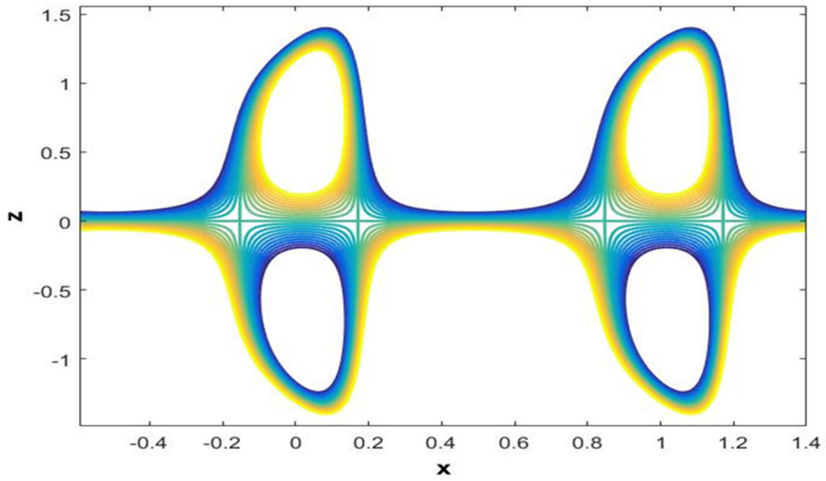


Figure 10. The trapping phenomenon occurs at $\beta = 0.4$. This results in an increase in the size of the bolus trapped which describes the volume of the fluid.

4. Conclusions

The present study investigates the effects of heat and mass transfer, thermal radiation, magnetic field, and channel inclination on the peristaltic flow of a Rabinowitsch fluid in an inclined symmetric channel under the assumptions of long-wavelength and low-Reynolds-number.

The results demonstrate that the flow characteristics are significantly influenced by the governing physical parameters. It is observed that the Hartmann number introduces a resistive Lorentz force, which modifies the velocity profile across the channel. The gravitational parameter enhances the fluid motion, while the inclination angle alters the flow distribution along the channel.

Thermal radiation and the heat source/sink parameter play an important role in both the temperature and concentration fields. Specifically, an increase in thermal radiation leads to an increase in both temperature and concentration, whereas, in the case of a heat sink, an increase in the parameter results in a decrease in both temperature and concentration. Furthermore, the pressure rise and frictional force exhibit directional dependence with respect to the flow rate, indicating the complex nature of peristaltic transport. The obtained solutions satisfy the imposed boundary conditions and show physically consistent behavior.

From an engineering perspective, the results highlight the importance of controlling magnetic, thermal, and geometrical parameters to optimize transport processes in peristaltic systems. These findings are relevant to biomedical applications, microfluidic devices, and industrial heat transfer systems.

The volume of the trapped bolus increases as the Hartmann number and the ratio of relaxation to retardation times increase, while it decreases as the heat source increases. Future studies may consider the inclusion of porous media, unsteady flow conditions, and experimental validation to further enhance the applicability of the model.

Author Contributions: H.S.G.: Her role in the research was as follows: She carried out the work conceptualization, methodology, validation, funding and investigating. L.G.A.: Her role in the research was as follows: She carried out the work's formal analysis, original draft preparation, writing, review and editing. All authors have read and agreed to the published version of the manuscript.

Funding: This research was funded by the authors.

Data Availability Statement: No datasets were generated or analyzed during the current study.

Acknowledgments: The authors would like to acknowledge the Deanship of Graduate Studies and Scientific Research, Taif University for funding this work.

Conflicts of Interest: The authors declare no conflicts of interest.

Abbreviations

$\bar{u}, \bar{v}$	Fluid velocity components
a	Channel half-width
b	Amplitude of the peristaltic wave
λ	Wavelength
c	constant speed
C_p	Specific heat
K	Thermal conductivity
α	Strength of the applied magnetic field aligned with the flow
ρ	Density of the fluid
Re	Reynolds number
F	Volume flow rate
g	Acceleration due to gravity
P	Pressure
θ	Fluid temperature
β_c	Concentration expansion coefficient
M	Hartman number
λ_1	The relaxation-to-retardation time ratio
F_λ	Friction force
K_T	Thermal expansion coefficient
D_m	Mass diffusion coefficient
Θ	Concentration
ε	Wave Amplitude Ratio

References

1. Abd-Alla, A.M.; Abo-Dahab, S.M.; Abdelhafez, M.A.; Elmhedy, Y. Effect of heat and mass transfer on the nanofluid of peristaltic flow in a ciliated tube. *Sci. Rep.* **2023**, *13*, 16008. [CrossRef]
2. Abd-Alla, A.M.; Abo-Dahab, S.M.; Thabet, E.N.; Abdelhafez, M.A. Peristaltic pump with heat and mass transfer of a fractional second grade fluid through porous medium inside a tube. *Sci. Rep.* **2022**, *12*, 10608. [CrossRef]
3. Alrashdi, A. Modelling and Analysis of Peristaltic Flows of Nanofluids and Hybrid Nanofluids for Heat Transfer Applications. Ph.D. Thesis, University of Leicester, Leicester, UK, 2024.

4. Bilal, M.; Javid, K.; Ali, N. Unsteady flow of hybrid fluid via peristaltic pumping in a wavy micro-channel under electric and magnetic field effects: An application of Hall device and slip boundary. *Proc. Inst. Mech. Eng. E J. Process Mech. Eng.* **2023**, *237*, 2157–2170. [CrossRef]
5. Chen, Z.; Zhu, L.-T.; Luo, Z.-H. Characterizing flow and transport in biological vascular systems: A review from physiological and chemical engineering perspectives. *Ind. Eng. Chem. Res.* **2024**, *63*, 4–36. [CrossRef]
6. Esser, F.; Masselter, T.; Speck, T. Silent pumpers: A comparative topical overview of the peristaltic pumping principle in living nature, engineering, and biomimetics. *Adv. Intell. Syst.* **2019**, *1*, 1900009. [CrossRef]
7. Farooq, S.; Shoaib, T.; Ravikumar, S.; Alotaibi, H. Thermal and concentration analysis of peristaltically driven motion of micro-rotating materials in a curved conduit influenced by slip and buoyant forces. *J. Sci. Technol.* **2025**, *60*, 1920–1934. [CrossRef]
8. Hasan, M.M. Numerical Study on Peristaltic Motion of Non-Newtonian Fluid in Physiology and Industry. Ph.D. Thesis, University of Dhaka, Dhaka, Bangladesh, 2024.
9. Khan, M.I.; Lashin, M.M.; Khedher, N.B.; Ahmed, B.; Khan, S.U.; Oreijah, M.; Galal, A.M. Peristaltic phenomenon in an asymmetric channel subject to inclined magnetic force and porous space. *Biomimetics* **2022**, *9*, 588. [CrossRef] [PubMed]
10. Magdy, M.M.; Nasr, A.G.; Abumandour, R.M. Effect of heat transfer and slipping on MHD peristaltic flow with suspended particles. *Eur. Eng. Res. J.* **2024**, *47*, 281–305. [CrossRef]
11. Magdy, M.; Nasr, A.G.; Abumandour, R.M.; El-Shorbagy, M.A. The impact of heat transfer and a magnetic field on peristaltic transport with slipping through an asymmetrically inclined channel. *J. Mech.* **2024**, *12*, 1827. [CrossRef]
12. Mohamed, R.; Abo-Dahab, S.; Abd-Alla, A.; Soliman, M. Magnetohydrodynamic double-diffusive peristaltic flow of radiating fourth-grade nanofluid through a porous medium with viscous dissipation and heat generation/absorption. *Sci. Rep.* **2023**, *13*, 13096. [CrossRef]
13. Hayat, T.; Iqbal, Z.; Alsaedi, A.; Asghar, S. Effect of thermal radiation on peristaltic flow of a non-Newtonian fluid in a channel. *Appl. Math. Mech.* **2014**, *35*, 1117–1130.
14. Akbar, N.S.; Nadeem, S. Influence of thermal radiation on peristaltic flow of a nanofluid in an asymmetric channel. *Int. J. Heat Mass Transf.* **2012**, *55*, 7234–7241.
15. Ellahi, R.; Riaz, A.; Nadeem, S.; Ali, M. Peristaltic flow of non-Newtonian fluid with heat and mass transfer in the presence of thermal radiation. *J. Mol. Liq.* **2013**, *189*, 132–138.
16. Sanil, P.; Gudekote, M.; Choudhari, R.; M R, M.; Vaidya, H.; Prasad, K.V. Entropy generation optimisation on the peristaltic mechanism of non-Newtonian Ree–Eyring fluid with variable liquid properties. *Bull. Viscous Process.* **2025**, *1*, 143. [CrossRef]
17. Takagi, D.; Balmforth, N.; Smith, S.G.L. Peristaltic pumping down a porous conduit. *J. Fluid Mech.* **2024**, *987*, A22. [CrossRef]
18. Tanveer, A.; Ashraf, M.B. Mixed convective flow of Sisko nanofluids over a curved surface with entropy generation and Joule heating. *Arab. J. Sci. Eng.* **2023**, *48*, 11263–11275. [CrossRef]
19. Tanveer, A.; Ashraf, M.B.; Masood, M. Entropy analysis of peristaltic flow over a curved channel under the impact of MHD and convective conditions. *Numer. Heat Transf. B Fundam.* **2024**, *85*, 45–57. [CrossRef]
20. Tanveer, A.; Ashraf, M.B.; Zaib-Un-Nisa. Analysis of entropy generation and Joule heating effects for MHD peristaltic flow over an asymmetric channel with mixed convective conditions. *Z. Angew. Math. Mech.* **2024**, *104*, e202300089. [CrossRef]
21. Ul-Haq, S.; Tanveer, A.; Ashraf, M.B.; Nawaz, R. Artificial neural network (ANN) analysis of non-similar solution of MHD nanofluid flow past a curved stretching surface. *Numer. Heat Transf. A Appl.* **2023**, *86*, 2399–2422. [CrossRef]
22. Vaidya, H.; Prasad, K.V.; Tripathi, D.; Choudhari, R.; Hanumantha; Ahmad, H. Viscoplastic hybrid nanofluids flow through a vertical stenosed artery. *BioNanoScience* **2023**, *13*, 2348–2370. [CrossRef]
23. Vaidya, H.; Rajashekhar, C.; Manjunatha, G.; Prasad, K.V. Effect of variable liquid properties on peristaltic flow of a Rabinowitsch fluid in an inclined convective porous channel. *Eur. Phys. J. Plus* **2019**, *134*, 231. [CrossRef]
24. Vaidya, H.; Shivaleela, S.; Rajashekhar, C.; Prasannakumara, B.C.; Kumar, R.N.; Gireesha, B.J. Scrutiny of MHD impact on Carreau–Yasuda (CY) fluid flow over a heated wall of a uniform microchannel. *Chin. J. Phys.* **2024**, *87*, 766–781. [CrossRef]
25. Vaidya, H.; Tripathi, D.; Khan, M.I.; Nasr, A.; Rajashekhar, C.; Prasad, K.V.; Khan, S.U. Analysis of peristaltic transport in the flow of non-Newtonian fluid with modified Darcy's law. *J. Non-Newton. Fluid Mech.* **2024**, *325*, 105214.
26. Vlahovska, P.M. Electrohydrodynamics of drops and vesicles. *Annu. Rev. Fluid Mech.* **2019**, *51*, 305–330. [CrossRef]
27. Zhang, L.; Bhatti, M.; Michaelides, E.E. Thermally developed coupled stress particle–fluid motion with mass transfer and peristalsis. *J. Therm. Anal. Calorim.* **2021**, *143*, 2514–2524. [CrossRef]
28. Thoubaan, M.G.; Al-Khafajy, D.G.S.; Wanas, A.K.; Breaz, D.; Cotîrlă, L.-I. Analysis of a bifurcation and stability of equilibrium points for Jeffrey fluid flow through a non-uniform channel. *Symmetry* **2024**, *16*, 1144. [CrossRef]
29. Halouani, B.; Nowar, K. Viscous dissipation and mixed convection effects on the induced magnetic field for peristaltic flow of a Jeffrey nanofluid. *Symmetry* **2024**, *16*, 329. [CrossRef]
30. Khan, A.A.; Zahra, B.; Ellahi, R.; Sait, S.M. Analytical solutions of peristalsis flow of non-Newtonian Williamson fluid in a curved micro-channel under the effects of electro-osmotic and entropy generation. *Symmetry* **2023**, *15*, 889. [CrossRef]

31. Abuasbeh, K.; Ahmed, B.; Niazi, A.U.K.; Awadalla, M. Entropy generation for MHD peristaltic transport of non-Newtonian fluid in a horizontal symmetric divergent channel. *Symmetry* **2023**, *15*, 359. [CrossRef]
32. Fatima, N.; Ijaz, N.; Riaz, A.; Tag El-Din, E.M.; Ali, S.S. Evaluation of asymmetric peristaltic pumping of drug-carrying fluid in a biological system: Multiphase flow analysis in biomedical applications. *Symmetry* **2022**, *14*, 2437. [CrossRef]
33. Elmhedy, Y.; Abd-Alla, A.M.; Abo-Dahab, S.M.; Alharabi, F.M.; Abdelhafez, M.A. Influence of inclined magnetic field and heat transfer on the peristaltic flow of Rabinowitsch fluid model in an inclined channel. *Sci. Rep.* **2024**, *14*, 4735. [CrossRef]
34. Abidin, M.Z.; Ullah, N.; Hussain, A.; Saadaoui, S.; Mohamed, M.M.I.; Deifalla, A. Case study of entropy optimization with the flow of Non-Newtonian nanofluid past converging conduit with slip mechanism: An application of geothermal engineering. *Case Stud. Therm. Eng.* **2023**, *52*, 103764. [CrossRef]
35. Abidin, M.Z.; Chen, J. Global well-posedness of generalized rotating magneto-hydrodynamics equations in variable expansion Fourier-Besov space. *J. Appl. Anal. Comput.* **2022**, *38*, 2187–2198. [CrossRef]
36. Shaheen, S.; Huang, H.; Al-Yarimi, F.A.; Arain, M.B. Theoretical analysis of Ellis fluid flow in two layers due to metachronal propulsion subject to heat and mass transfer: Application in biological function. *Case Stud. Therm. Eng.* **2024**, *59*, 104446. [CrossRef]
37. Abdelhafez, M.A.; Abd-Alla, A.M.; Abo-Dahab, S.M.; Elmhedy, Y. Influence of an inclined magnetic field and heat and mass transfer on the peristaltic flow of blood in an asymmetric channel. *Sci. Rep.* **2023**, *13*, 5749. [CrossRef]
38. Adnan, F.A.; Abdul Hadi, A.M. Effect of an inclined magnetic field on peristaltic flow of Bingham plastic fluid in an inclined symmetric channel with slip condition. *Iraqi J. Sci.* **2019**, *60*, 1551–1574. [CrossRef]

Disclaimer/Publisher's Note: The statements, opinions and data contained in all publications are solely those of the individual author(s) and contributor(s) and not of MDPI and/or the editor(s). MDPI and/or the editor(s) disclaim responsibility for any injury to people or property resulting from any ideas, methods, instructions or products referred to in the content.